

Chaotic Geodesics*

Jean-Luc Thiffeault

Department of Mathematics, University of Wisconsin, Madison, WI 53706, USA[†]

Khalid Kamhawi

Department of Mathematics, Imperial College London, London, SW7 2AZ, UK

(Dated: 26 November 2007)

When a shallow layer of inviscid fluid flows over a substrate, the fluid particle trajectories are, to leading order in the layer thickness, geodesics on the two-dimensional curved space of the substrate. Since the two-dimensional geodesic equation is a two degree-of-freedom autonomous Hamiltonian system, it can exhibit chaos, depending on the shape of the substrate. We find chaotic behaviour for a range of substrates.

Keywords: shallow water flows; chaotic advection; particle transport

I. INTRODUCTION

Many well-known physical systems take the form of geodesic flow on a manifold. For instance, Euler's equation can be thought of as a geodesic flow in the space of volume-preserving diffeomorphisms, [1–6] and free rigid body motion as geodesic flow in $SO(3)$. In both cases, the metric on the space corresponds to the kinetic energy norm. It is also known that the *geodesic deviation equation* [7] describes the stability of such flows. For instance, a space of negative curvature will lead to divergence of trajectories, and hence to chaos if the space is compact. But compact spaces of strictly negative curvature are hard to come by in the real world, to say the least. If we expect the negative curvature to lead to chaotic geodesics, we are better off looking for spaces with non-sign-definite curvature, but such that the averaging of the curvature over trajectories leads to chaos (*i.e.*, the negative curvature ‘wins’).

In this contribution we will discuss a system which is physically-motivated and leads to chaotic geodesics. This system is the flow of a shallow layer of ideal, irrotational fluid on a curved substrate. Following Rienstra [8], we will show that, to leading order, the governing equation can be solved in terms of characteristics. Moreover, the characteristics are geodesics on the curved substrate, possibly modified by gravity if it is present.

Of course, the chaotic trajectories have a nasty tendency to cross and form caustics everywhere. Hydrodynamically, caustics are usually manifested as hydraulic jumps or so-called ‘mass tubes,’ [9] visible as a thicker edge region of the fluid in Fig. 1 (top). Edwards *et al.* [9] have recently described these mass tubes using the theory of ‘delta-shocks.’ [9–13] At this point, we are unable to apply this theory to our problem, which means that solutions be-

*To appear in Proceedings of the conference on *Chaos, Complexity, and Transport: Theory and Applications* (Le Pharo, Marseille, June 2007).

[†]Electronic address: jeanluc@math.wisc.edu

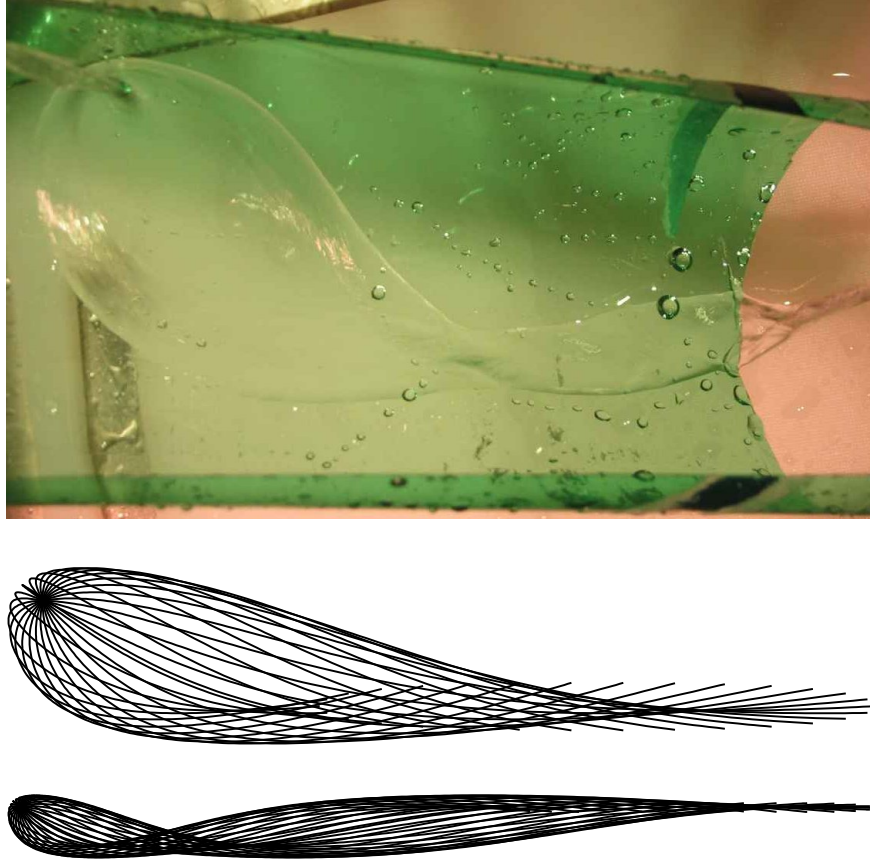


FIG. 1: Experiment in the kitchen sink, using a cut-open plastic bottle (top). The jet from the faucet impacts the inclined bottle. The pattern is qualitatively well reproduced by following fluid trajectories emanating from a point source on a cylinder (middle). However, if we pursue the trajectories further (bottom), the ideal theory presented here predicts that the flow should crawl back up the side to the same initial height. The discrepancy is clearly due to dissipation.

come dubious after characteristics begin to cross. Unfortunately, since our characteristics are chaotic, they tend to cross a lot. Nevertheless, we believe that studying the basic properties of this geodesic flow is worthwhile as a first stab at describing the transport properties of flows on curved substrates. In addition, the geodesic flow we present is an interesting mathematical system, with rich dynamics that deserve to be studied on their own.

Having gotten these disclaimers out of the way, let us proceed with the analysis. We shall do this in stages. In Section II we introduce a curved non-orthogonal coordinate system to describe the substrate, singling out a direction normal to the substrate. In Section III we use this direction to expand our fluid equations and derive a shallow-layer form. We show that the resulting equation can be solved in terms of characteristics, which are geodesics on the two-dimensional curved substrate, modified by gravity. In Section IV we look at specific numerical solutions for particle trajectories, and in Section V we speculate on their chaotic nature. We offer some closing comments in Section VI.

II. COORDINATE SYSTEM

A. Separating the Shallow Direction

In our problem, fluid motion occurs over a curved substrate of arbitrary shape. The direction normal to the substrate is special in that it defines the direction in which the fluid layer is assumed ‘shallow.’ Hence, it is convenient to locate a point \mathbf{r} in the fluid as

$$\mathbf{r}(x^1, x^2, y) = \mathbf{X}(x^1, x^2) + y \hat{\mathbf{e}}_3(x^1, x^2) \quad (1)$$

where $\mathbf{X}(x^1, x^2)$ is the location of the substrate, $\hat{\mathbf{e}}_3$ is a unit vector normal to the substrate, and y is the perpendicular distance from \mathbf{r} to the substrate. The coordinates x^1 and x^2 are substrate coordinates used to localise points on the substrate. For example, in Section II B we will use the Monge parametrisation, $\mathbf{X} = (x^1 \ x^2 \ f(x^1, x^2))^T$, where f gives the height of the substrate.

The tangent vectors to the substrate are

$$\mathbf{e}_\alpha := \partial_\alpha \mathbf{X} \quad (2)$$

where $\partial_\alpha := \partial/\partial x^\alpha$. The coordinate vectors associated with the coordinate system are found from (1),

$$\tilde{\mathbf{e}}_\alpha := \partial_\alpha \mathbf{r} = \mathbf{e}_\alpha + \mathcal{O}(y), \quad \hat{\mathbf{e}}_3 := \frac{\partial \mathbf{r}}{\partial y}. \quad (3)$$

where Greek indices only take the value 1 or 2. Note that the \mathbf{e}_α are not necessarily orthogonal or normalised.

We adopt the convention that quantities with a tilde are evaluated in the ‘bulk’ (away from the substrate), and thus depend on y , whilst those without the tilde are ‘substrate’ quantities and do not depend on y . Thus, $\tilde{\mathbf{e}}_\alpha(x^1, x^2, 0) = \mathbf{e}_\alpha(x^1, x^2)$. The three-dimensional metric tensor $\tilde{\mathbf{g}}_{ab}$ has components

$$\tilde{\mathbf{g}}_{\alpha\beta} := \tilde{\mathbf{e}}_\alpha \cdot \tilde{\mathbf{e}}_\beta = \tilde{\mathbb{G}}_{\alpha\beta}, \quad \tilde{\mathbf{g}}_{\alpha 3} := \tilde{\mathbf{e}}_\alpha \cdot \hat{\mathbf{e}}_3 = 0, \quad \tilde{\mathbf{g}}_{33} := \hat{\mathbf{e}}_3 \cdot \hat{\mathbf{e}}_3 = 1,$$

where

$$\begin{aligned} \tilde{\mathbb{G}}_{\alpha\beta} &:= \tilde{\mathbf{e}}_\alpha \cdot \tilde{\mathbf{e}}_\beta = \mathbb{G}_{\alpha\beta} + \mathcal{O}(y), \\ \mathbb{G}_{\alpha\beta} &:= \mathbf{e}_\alpha \cdot \mathbf{e}_\beta. \end{aligned} \quad (4)$$

The three-dimensional metric tensor is thus block-diagonal, and the y coordinate is unstretched compared to the Cartesian coordinate system. It measures the true perpendicular distance from the substrate to a point in the fluid.

Given the substrate vectors \mathbf{e}_α , it is easy to solve for the covectors \mathbf{e}^α , which are such that $\mathbf{e}^\alpha \cdot \mathbf{e}_\beta = \delta_\beta^\alpha$. Then the bulk covectors are

$$\tilde{\mathbf{e}}^\alpha = \mathbf{e}^\alpha + \mathcal{O}(y), \quad (5)$$

to leading order in y . From (5), we find the inverse metrics,

$$\begin{aligned} \tilde{\mathbb{G}}^{\alpha\beta} &= \tilde{\mathbf{e}}^\alpha \cdot \tilde{\mathbf{e}}^\beta = \mathbb{G}^{\alpha\beta} + \mathcal{O}(y), \\ \mathbb{G}^{\alpha\beta} &= \mathbf{e}^\alpha \cdot \mathbf{e}^\beta. \end{aligned} \quad (6)$$

Higher-order terms in y will not be needed.

B. Substrate Coordinates

For most applications in the literature of thin films and shallow layers, orthonormal coordinates have been the coordinates of choice. This is because the main substrate shapes that have been treated are planes, cylinders, and spheres, where orthonormal coordinates are readily available. For a general substrate shape, orthonormal coordinates are difficult to construct and require numerical integration. Singularities (umbilics) also cause problems. [14] For our application—flow down a curved substrate—the Monge representation of a surface [15] is the most convenient.

The Monge representation is a glorified name for a parametrisation of the substrate by

$$\mathbf{X}(x^1, x^2) = (x^1 \ x^2 \ f(x^1, x^2))^T \quad (7)$$

in three-dimensional Cartesian space. Following standard notation, [15] we define

$$p = \partial_1 f, \quad q = \partial_2 f, \quad (8a)$$

$$r = \partial_1 \partial_1 f, \quad s = \partial_1 \partial_2 f, \quad t = \partial_2 \partial_2 f. \quad (8b)$$

The unnormalised, nonorthogonal tangents \mathbf{e}_1 and \mathbf{e}_2 are

$$\mathbf{e}_1 = \partial_1 \mathbf{X} = (1 \ 0 \ p)^T, \quad \mathbf{e}_2 = \partial_2 \mathbf{X} = (0 \ 1 \ q)^T,$$

and their normalised cross product gives the normal to the substrate,

$$\hat{\mathbf{e}}_3 = \frac{1}{w} (-p \ -q \ 1)^T.$$

The corresponding covectors are

$$\mathbf{e}^1 = \frac{1}{w^2} ((1 + q^2) \ -pq \ p)^T, \quad \mathbf{e}^2 = \frac{1}{w^2} (-pq \ (1 + p^2) \ q)^T$$

and $\hat{\mathbf{e}}_3$ is its own covector. The metric tensor of the substrate and its inverse are

$$\{\mathbb{G}_{\alpha\beta}\} = \mathbf{e}_\alpha \cdot \mathbf{e}_\beta = \begin{pmatrix} 1 + p^2 & pq \\ pq & 1 + q^2 \end{pmatrix}, \quad (9a)$$

$$\{\mathbb{G}^{\alpha\beta}\} = \mathbf{e}^\alpha \cdot \mathbf{e}^\beta = \frac{1}{w^2} \begin{pmatrix} 1 + q^2 & -pq \\ -pq & 1 + p^2 \end{pmatrix}, \quad (9b)$$

with determinant

$$w = (\det \mathbb{G}_{\alpha\beta})^{1/2} = \sqrt{1 + p^2 + q^2}.$$

Finally, we will need the Christoffel symbols $\Gamma_{\alpha\beta}^\sigma$, defined by

$$\Gamma_{\alpha\beta}^\sigma = \frac{1}{2} \mathbb{G}^{\sigma\gamma} (\partial_\alpha \mathbb{G}_{\gamma\beta} + \partial_\beta \mathbb{G}_{\gamma\alpha} - \partial_\gamma \mathbb{G}_{\alpha\beta}) \quad (10)$$

and in Monge coordinates given by

$$\Gamma_{\alpha\beta}^1 = \frac{p}{w^2} \begin{pmatrix} r & s \\ s & t \end{pmatrix}, \quad \Gamma_{\alpha\beta}^2 = \frac{q}{w^2} \begin{pmatrix} r & s \\ s & t \end{pmatrix}. \quad (11)$$

The Christoffel symbols arise when taking covariant derivatives. [7, 16, 17] Note that in (10) we used the usual convention that repeated indices are summed.

We write the normalised gravity vector as

$$\mathbf{g} = (\sin \theta \cos \phi \quad \sin \theta \sin \phi \quad -\cos \theta)^T, \quad (12)$$

so that the inclination angle θ is zero for gravity pointing downwards, and for $\phi \in (-\pi/2, \pi/2)$ positive θ induces flow in the positive x^1 direction. Then we have the components

$$\begin{aligned} g_s^1 &= \mathbf{g} \cdot \mathbf{e}^1 = -(p \cos \theta + pq \sin \theta \sin \phi - (1 + q^2) \sin \theta \cos \phi) / w^2, \\ g_s^2 &= \mathbf{g} \cdot \mathbf{e}^2 = -(q \cos \theta + pq \sin \theta \cos \phi - (1 + p^2) \sin \theta \sin \phi) / w^2, \end{aligned} \quad (13)$$

The specific parametrisation of the substrate introduced in this section will not be needed in the derivation of the equations of motion (Section III), only in their solution. Hence, a different parametrisation could be used if called for by the geometry of the substrate. For instance, flow down a curved filament is better parametrised by cylindrical coordinates, or if the substrate has overhangs (making f multivalued) coordinates based on arc length are preferable.

III. EQUATIONS OF MOTION

Now that we've set up an appropriate coordinate system on our curved substrate, we need some dynamical equations of motion for the fluid. We assume an inviscid, irrotational fluid with a free surface at $y = \eta(x^1, x^2)$, with slip boundary conditions at the substrate $y = 0$. The pressure on the free surface is assumed constant (zero). We also assume the flow is steady and irrotational, so that the velocity can be written in terms of a scalar potential, $\mathbf{u} = \nabla \varphi$. The equations satisfied by the fluid are then

$$\nabla^2 \varphi = 0, \quad \text{mass conservation;} \quad (14a)$$

$$\frac{1}{2} |\nabla \varphi|^2 + \frac{p}{\rho} - \mathbf{g} \cdot \mathbf{r} = H, \quad \text{Bernoulli's law;} \quad (14b)$$

where H is a constant, with boundary conditions

$$\partial_y \varphi = 0 \quad \text{at } y = 0, \quad \text{no-throughflow at substrate;} \quad (15a)$$

$$\nabla \varphi \cdot \nabla \eta = \partial_y \varphi \quad \text{at } y = \eta, \quad \text{kinematic condition at free surface;} \quad (15b)$$

$$p = 0 \quad \text{at } y = \eta, \quad \text{constant pressure at free surface.} \quad (15c)$$

In terms of our curvilinear coordinates, equation (14b) becomes

$$\tilde{\mathbb{G}}^{\alpha\beta} \partial_\alpha \varphi \partial_\beta \varphi + (\partial_y \varphi)^2 + \frac{2p}{\rho} - 2\mathbf{g} \cdot \mathbf{r} = 2H. \quad (16)$$

A. Small-parameter Expansion

Now we assume that the fluid layer is shallow, so that y is proportional to ε . After replacing y by εy , Eq. (14b) becomes

$$(\mathbb{G}^{\alpha\beta} + \mathcal{O}(\varepsilon)) \partial_\alpha \varphi \partial_\beta \varphi + \varepsilon^{-2} (\partial_y \varphi)^2 + \frac{2p}{\rho} - 2\mathbf{g} \cdot (\mathbf{X} + \varepsilon y \hat{\mathbf{e}}_3) = 2H. \quad (17)$$

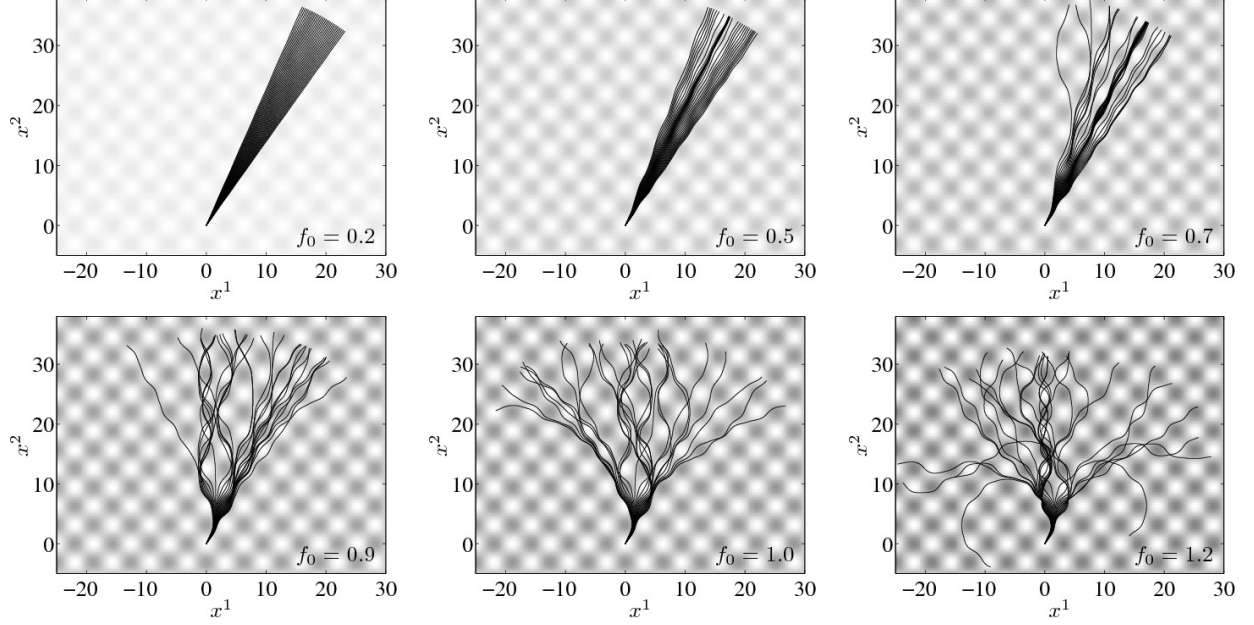


FIG. 2: A pencil of 30 trajectories starting from the origin at different angles, each with initial kinetic energy $1/2$. The substrate has shape $f(x^1, x^2) = f_0 \cos x^1 \cos x^2$, and the plots are for different values of f_0 . Gravity is turned off: $g = 0$. The grey background shows the periodicity of the substrate.

We also expand φ in powers of ε ,

$$\varphi(x^1, x^2, y) = \varphi_{(0)} + \varepsilon \varphi_{(1)} + \varepsilon^2 \varphi_{(2)} + \dots \quad (18)$$

The leading-order term in (17) occurs at order ε^{-2} , and gives $\partial_y \varphi_{(0)} = 0$. Hence, we have $\varphi_{(0)} = \Phi(x^1, x^2)$ independent of y . The next nontrivial terms are at order ε^0 ,

$$\mathbb{G}^{\alpha\beta} \partial_\alpha \Phi \partial_\beta \Phi + (\partial_y \varphi_{(1)})^2 + \frac{2p}{\rho} - 2\mathbf{g} \cdot \mathbf{X} = 2H. \quad (19)$$

We evaluate the whole of (19) at $y = 0$, and use the boundary conditions (15a) and (15c),

$$\mathbb{G}^{\alpha\beta} \partial_\alpha \Phi \partial_\beta \Phi - 2\mathbf{g} \cdot \mathbf{X} = 2H. \quad (20)$$

This is the equation that we need to solve to find the leading-order velocity potential $\Phi(x^1, x^2)$. We discuss the method of solution in the next section. Note that we will not need to solve the mass conservation equation (14a): at leading order, it only serves to find the fluid height once the velocity field is obtained.

B. Solution in Terms of Characteristics

As pointed out by Rienstra, [8] the trick to solving Eq. (20) is to use the method of characteristics. To do this, we differentiate (20) with respect to x^γ , which gets rid of the constant H ,

$$2\mathbb{G}^{\alpha\beta} \partial_\alpha \Phi \partial_\gamma \partial_\beta \Phi + \partial_\gamma \mathbb{G}^{\alpha\beta} \partial_\alpha \Phi \partial_\beta \Phi = 2\mathbf{g} \cdot \partial_\gamma \mathbf{X}. \quad (21)$$

The horizontal components of velocity are $\dot{x}^\alpha = \mathbb{G}^{\alpha\beta} \partial_\beta \Phi$, where the overdot denotes a time derivative; hence,

$$\partial_\gamma \partial_\beta \Phi = \partial_\beta (\mathbb{G}_{\gamma\delta} \dot{x}^\delta) = \mathbb{G}_{\gamma\delta} \partial_\beta \dot{x}^\delta + \partial_\beta \mathbb{G}_{\gamma\delta} \dot{x}^\delta. \quad (22)$$

From the chain rule, we have $\ddot{x}^\delta = \partial_\beta \dot{x}^\delta \dot{x}^\beta$; using this and (22) in (21), we find, after dividing by two,

$$\mathbb{G}_{\gamma\delta} \ddot{x}^\delta + \partial_\beta \mathbb{G}_{\gamma\delta} \dot{x}^\beta \dot{x}^\delta + \frac{1}{2} \partial_\gamma \mathbb{G}^{\alpha\beta} \mathbb{G}_{\alpha\delta} \mathbb{G}_{\beta\rho} \dot{x}^\delta \dot{x}^\rho = \mathbf{g} \cdot \mathbf{e}_\gamma. \quad (23)$$

Now we multiply by $\mathbb{G}^{\sigma\gamma}$, and obtain after an integration by parts and a bit of manipulation

$$\ddot{x}^\sigma + \Gamma_{\alpha\beta}^\sigma \dot{x}^\alpha \dot{x}^\beta = \mathbf{g} \cdot \mathbf{e}^\sigma \quad (24)$$

where the $\Gamma_{\alpha\beta}^\sigma$ are defined by (11). Equation (24) describes *geodesics* in the curved coordinates of the substrate, under the influence of gravity. In the absence of gravity, the fluid trajectories are essentially going in straight lines in the curved substrate coordinates. (In general relativity, unlike here, the gravity determines the curvature of space.)

If we define the *covariant derivative* of a vector V^σ along the trajectory [7, 16–18],

$$\frac{D}{D\tau} V^\sigma := \dot{V}^\sigma + \Gamma_{\alpha\beta}^\sigma \dot{x}^\alpha V^\beta, \quad (25)$$

where τ is the time (to avoid confusion with t in Eq. (8)), then the geodesic equation (24) takes the more intuitive form

$$\frac{D}{D\tau} \dot{x}^\sigma = \mathbf{g} \cdot \mathbf{e}^\sigma \quad (26)$$

which looks a lot like Newton's second law, but here it incorporates the constraint that fluid particles remain on the substrate.

Equation (24) is a two degree-of-freedom autonomous Hamiltonian system, with the energy H defined by equation (20) as an invariant. Hence, any other invariant will make the system integrable, and rule out chaos. In particular, a surface with a translational symmetry cannot exhibit chaos.

IV. FLUID PARTICLE TRAJECTORIES

To get a feel for the possible range of behaviour of fluid trajectories, we now solve the geodesic equation (24) for a range of substrates. We shall always use a set of fluid trajectories starting at the same spatial point, with the same initial kinetic energy but different direction. This models a point source, or a thin jet impacting the substrate.

First, following Rienstra [8] we solve the equations on a cylindrical substrate. Figure 1 (middle) shows some trajectories, all emanating from the same point. Qualitatively, the pattern captures well the observed behaviour of a jet (from a faucet) impacting the inside of a cut-out plastic bottle (Fig. 1, top). However, if we pursue the trajectories further (Fig. 1, bottom), we see that they crawl back up the side of the cylinder, with no loss of energy, in contrast to the experimental picture. This comes from neglecting the hydraulic jumps that occur, as well as viscosity. [9] Observe that the trajectories follow a very ordered pattern, and are definitely not chaotic. This is as expected, since there is a symmetry direction, and so the motion is integrable (Section III).

Next we move on to more complex substrates. Since there is basically an infinity of choices here, we limit ourselves to periodic substrates with shape

$$f(x^1, x^2) = f_0 \sin x^1 \sin x^2 \quad (27)$$

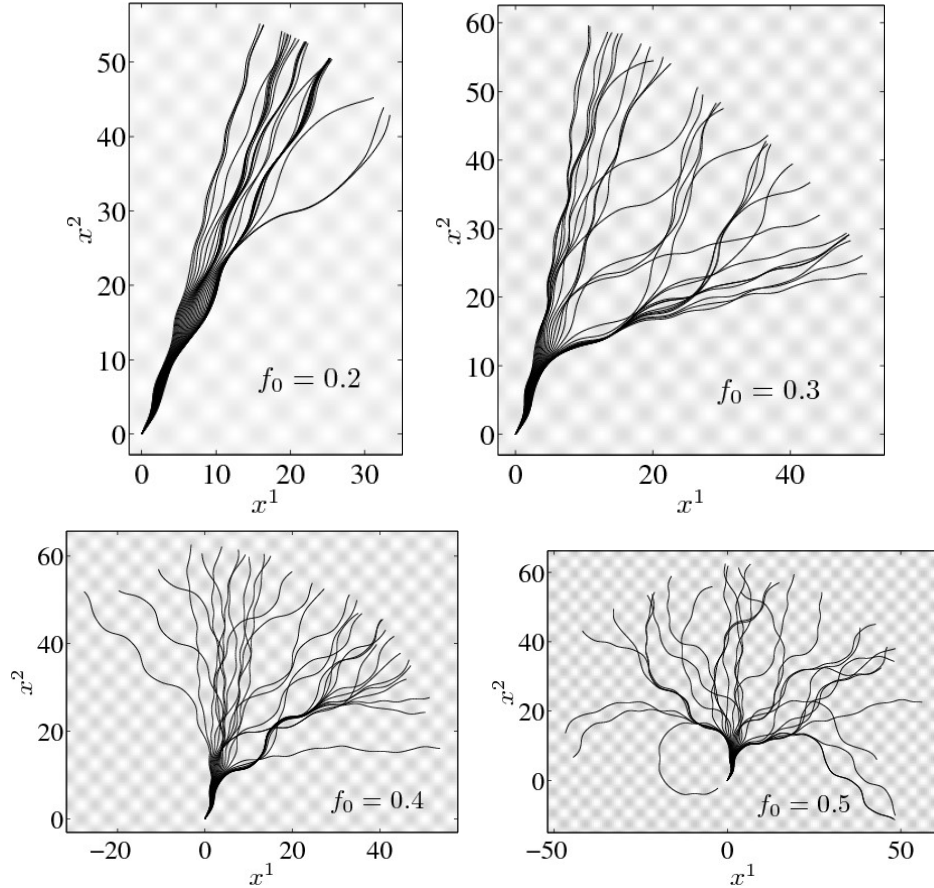


FIG. 3: Same parameters as in Fig. 2, but with gravity turned on: $g = 1$. The trajectories exhibit chaos-like behaviour for much lower substrate height, since they begin at the top of a bump and thus have potential energy to draw upon.

for various values of f_0 . The other variables in the system are the strength of gravity (which can be chosen as unity if it is not zero, by rescaling the substrate height) and its orientation (as given by the angles θ and ϕ in Eq. (12)).

Figure 2 shows a pencil of 30 trajectories starting from the origin at different angles, each with initial kinetic energy $1/2$, for different values of f_0 , in the absence of gravity. The first two cases display regular behaviour, but for substrate heights $f_0 = 0.7$ there is chaotic-like behaviour. These are, however, fairly extreme values of f_0 , corresponding to heavily-deformed substrates. Our expansion should be able to accommodate this, since the variations in the substrate height are not assumed small (only those in the fluid thickness are). For extreme heights ($f_0 = 1.2$, last case in Fig. 2), some trajectories actually backfire and come around the initial point.

Figure 3 shows results for the same parameters as Fig. 2, but with gravity $g = 1$. The inclination is nil ($\theta = 0$). It is clear that chaotic-like behaviour sets in for much smaller values of f_0 , even showing backscatter for $f_0 = 0.5$ in the last frame. This is because the fluid elements can now draw on the potential energy they inherit from starting at the top of the bump.

This suggests that, in the presence of gravity, the results should be substantially different

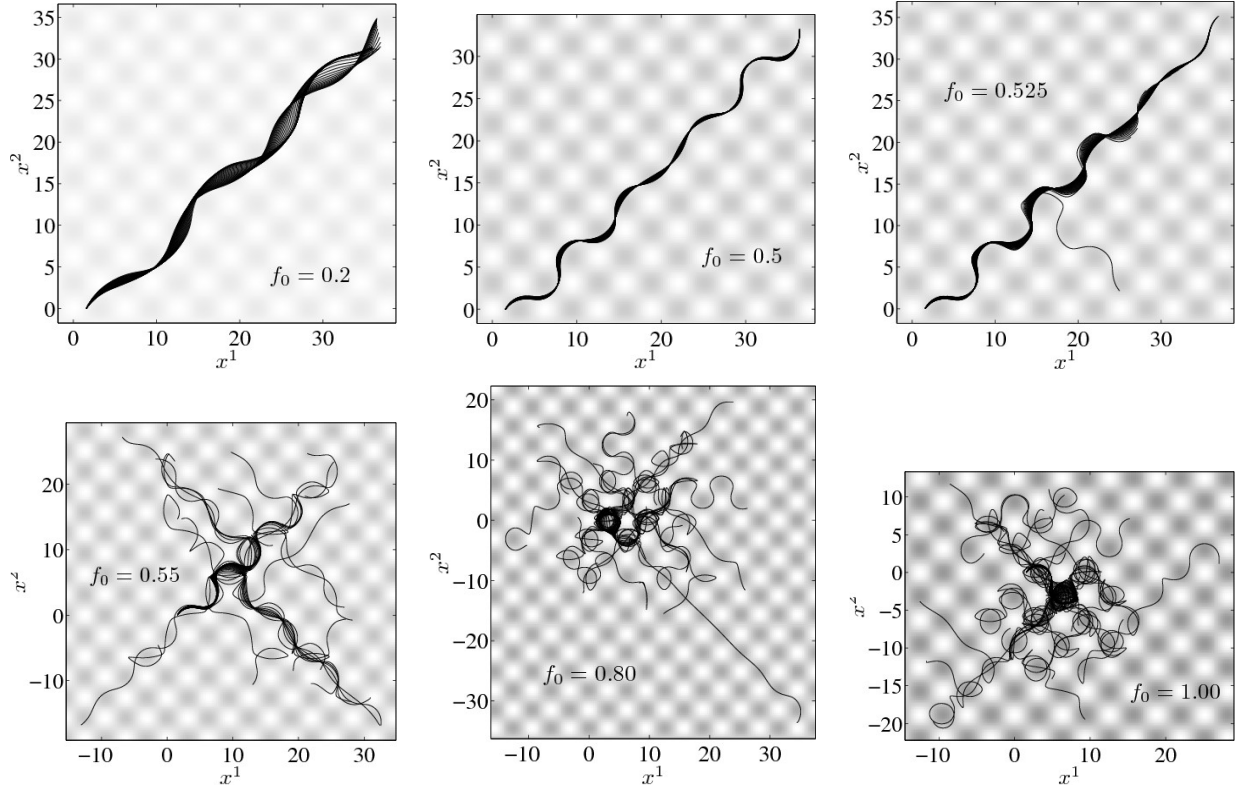


FIG. 4: Same parameters as in Fig. 3, but with initial condition $(x^1, x^2) = (\pi/2, 0)$. For larger substrate amplitudes, the system is dominated by ‘rimming,’ where particles skim a depression before moving to the next one, or sometimes undergo long flights.

if we start elsewhere on the substrate. Figure 4 shows simulations with the same parameters as in Fig. 3, but starting at $(x^1, x^2) = (\pi/2, 0)$, some way down the bump. The motion is then confined to narrow channels for moderate f_0 . But for larger substrate amplitudes, the system is dominated by ‘rimming,’ where particles skim a depression before moving to the next one, or sometimes undergo long flights. This is a similar situation to basketball (or golf), where the ball turns around the hoop (or cup) a while before deciding to go in or out. If we take an initial condition at the bottom of the bump, $(x^1, x^2) = (\pi, 0)$, then the trajectories do not have enough energy to escape the potential well (Fig. 5).

Finally, in Fig. 6 we illustrate the effect of inclining the substrate at an angle $\theta = \pi/8$. With $\phi = -\pi/2$ the trajectories flow ‘downhill,’ in the negative x^2 direction, modified by the bumps. The system still appears to become chaotic for larger f_0 . Larger bumps induce a ‘shadow’ effect, where they prevent fluid from flowing behind them (in particular for $f_0 = 0.6$).

V. LYAPUNOV EXPONENTS AND CHAOS

We now investigate whether the behaviour described in the previous section is chaotic or not. The first variation of the geodesic Eq. (24) gives

$$\delta \ddot{x}^\sigma + 2\Gamma_{\alpha\beta}^\sigma \dot{x}^\alpha \delta \dot{x}^\beta + \partial_\gamma \Gamma_{\alpha\beta}^\sigma \dot{x}^\alpha \dot{x}^\beta \delta x^\gamma = -\mathbf{g} \cdot \mathbf{e}^\tau \Gamma_{\gamma\tau}^\sigma \delta x^\gamma \quad (28)$$

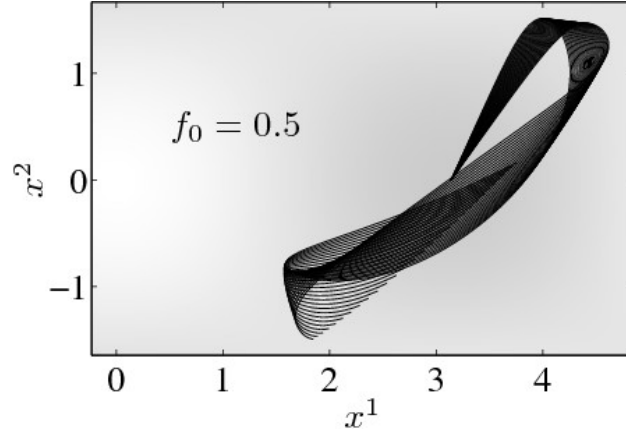


FIG. 5: Same parameters as in Fig. 3, but with initial condition $(x^1, x^2) = (\pi, 0)$. The particles begin at the bottom of the potential well, and they do not have the energy to escape.

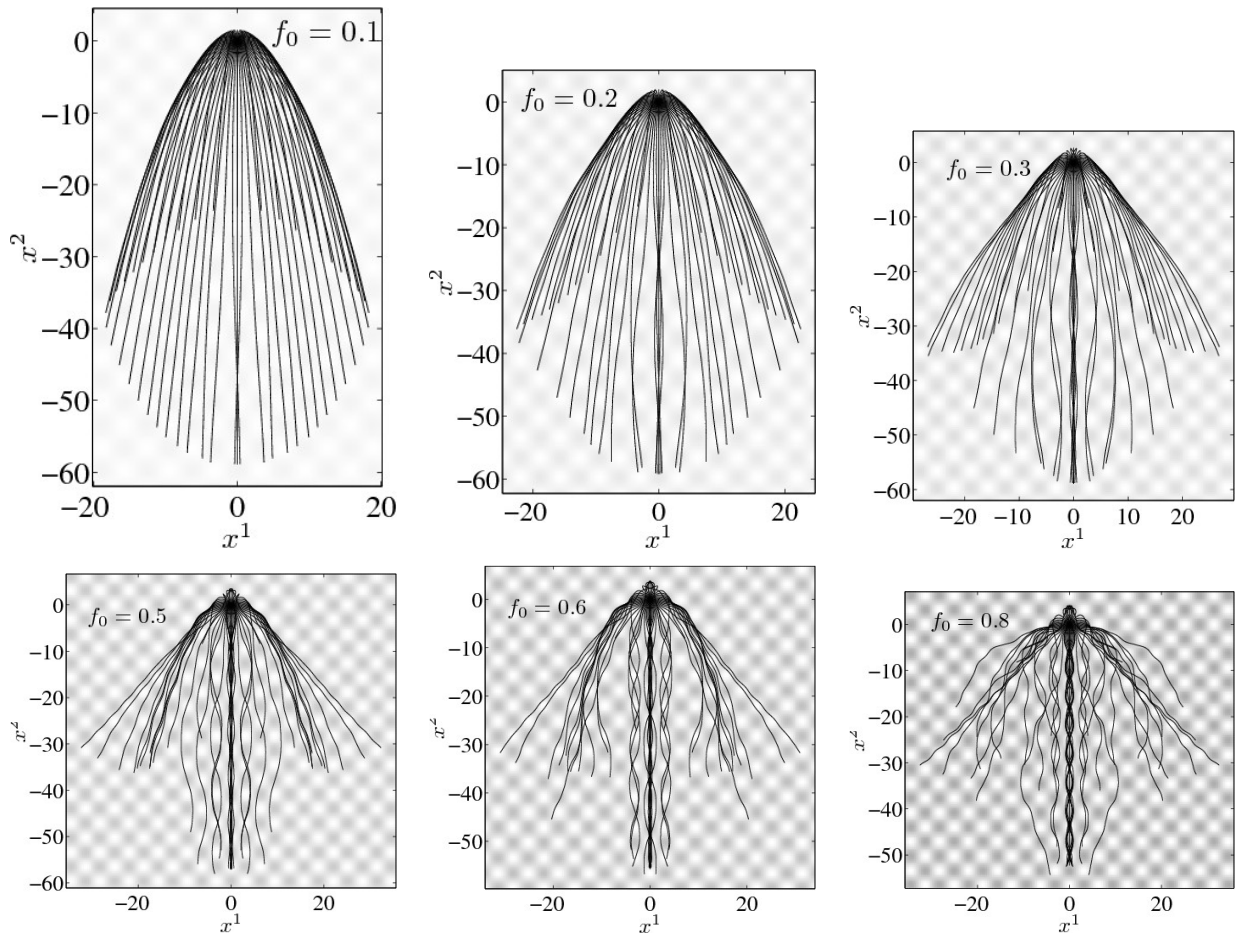


FIG. 6: Same parameters as in Fig. 3, but with incline $\theta = \pi/8$ and $\phi = -\pi/2$. For larger bumps there is a ‘shadow’ effect, particularly for $f_0 = 0.6$.

where we have used $\partial_\gamma e^\sigma = -\Gamma_{\gamma\tau}^\sigma e^\tau$. This equation can be massaged into the *geodesic deviation equation*, [7, 19]

$$\frac{D^2}{D\tau^2}\delta x^\sigma + R^\sigma{}_{\beta\gamma\alpha}\dot{x}^\alpha\dot{x}^\beta\delta x^\gamma = 0 \quad (29)$$

where $D/D\tau$ is defined in (25), and

$$R^\sigma{}_{\beta\gamma\alpha} := \partial_\gamma\Gamma_{\alpha\beta}^\sigma - \partial_\alpha\Gamma_{\gamma\beta}^\sigma + \Gamma_{\gamma\lambda}^\sigma\Gamma_{\alpha\beta}^\lambda - \Gamma_{\alpha\lambda}^\sigma\Gamma_{\gamma\beta}^\lambda \quad (30)$$

is the Riemann curvature tensor. For two-dimensional surfaces, the curvature tensor simplifies to

$$R^\sigma{}_{\beta\gamma\alpha} = \mathcal{G}(\delta^\sigma{}_\gamma\mathbb{G}_{\beta\alpha} - \delta^\sigma{}_\alpha\mathbb{G}_{\beta\gamma}) \quad (31)$$

where $\mathcal{G} = (rt - s^2)/w^4$ is the Gaussian curvature and $\mathbb{G}_{\beta\alpha}$ is given by Eq. (9). Hence, a simplified form of (28) for surfaces is

$$\frac{D^2}{D\tau^2}\delta x^\sigma + \mathcal{G}(\langle\dot{x}, \dot{x}\rangle\delta x^\sigma - \langle\dot{x}, \delta x\rangle\dot{x}^\sigma) = 0 \quad (32)$$

where the inner product is defined by $\langle V, W \rangle := \mathbb{G}_{\alpha\beta}V^\alpha W^\beta$.

Note that the gravitational term does not enter Eq. (28) directly, though it does through (24). For the rest of this discussion we will assume $g = 0$, since it simplifies the discussion considerably. If that is then case, then it is easy to show that

$$\frac{D}{D\tau}\langle\dot{x}, \delta x\rangle = \langle\dot{x}, \frac{D}{D\tau}\delta x\rangle, \quad \frac{D^2}{D\tau^2}\langle\dot{x}, \delta x\rangle = 0 \quad (33)$$

which means that if we choose the initial δx^α such that $\langle\dot{x}, \delta x\rangle = \langle\dot{x}, D\delta x/D\tau\rangle = 0$, then $\langle\dot{x}, \delta x\rangle$ remains zero for all time. With this choice initial condition, the geodesic deviation equation (32) finally takes the form

$$\frac{D^2}{D\tau^2}\delta x^\sigma + \mathcal{G}\langle\dot{x}, \dot{x}\rangle\delta x^\sigma = 0. \quad (34)$$

Now we can ask under what condition the substrate shape will be favourable to chaotic geodesics. Since Eq. (34) resembles an oscillator equation, and $\langle\dot{x}, \dot{x}\rangle \geq 0$, we see that negative Gaussian curvature will favour divergence of trajectories.

We have not yet solved Eq. (28) for δx^σ , but a comparison of the distance between two initially very close trajectories is shown in Fig. 7, for the same parameters as in Fig. 3 ($f_0 = 0.5$). Unsurprisingly, the plot confirms exponential growth, demonstrating at least numerically that chaos is indeed present.

VI. DISCUSSION

We have shown that the flow of a shallow layer of inviscid, irrotational fluid on a curved substrate leads to particle trajectories that follow geodesics in the curved space, subject to gravity. We have displayed the range of behaviour that these geodesics can exhibit, from regular to chaotic.

As Fig. 1 shows, the theory is not likely to be valid much beyond the point where characteristics cross, and viscosity also causes important corrections. Another effect we ignored

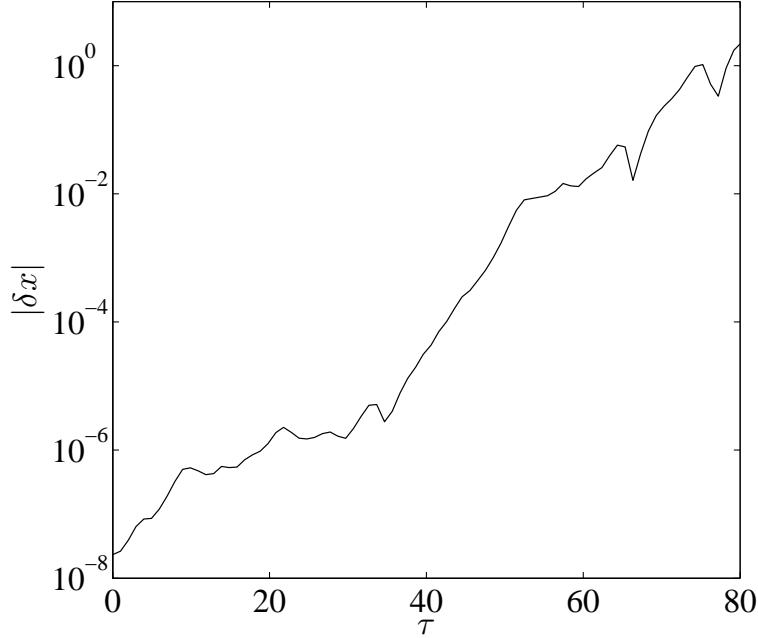


FIG. 7: The Cartesian distance $|\delta x|$ between two trajectories, for the same parameters as in Fig. 3 with $f_0 = 0.5$. The trajectories diverge extremely rapidly, consistent with chaotic behaviour.

is the possibility that centrifugal forces can cause the fluid to spin out and detach from the substrate. [9] Experiments are needed to determine to what extent the chaos observed here is reproduced in reality. If chaos is indeed prevalent, then perhaps chaotic advection can be exploited in some applications to enhance mixing in shallow layers.

We made the case in the introduction that chaos in the geodesic equations was a subject worthy of study on its own. The emergence of chaotic behaviour as a function of Gaussian curvature, as embodied by Eq. (32), should be a rich subject of study, in particular because of the simple form this equation takes on a surface.

We note in closing that a similar study can be made for viscous thin films. [20] However, trajectories there are much less prone to chaotic behaviour, because of the diminished role of inertia.

-
- [1] V. I. Arnold, *Ann. Inst. Fourier* **16**, 319 (1966).
 - [2] V. I. Arnold, *Usp. Mat. Nauk.* **24**, 225 (1969).
 - [3] V. I. Arnold, *Mathematical Methods of Classical Mechanics*, second edn. (Springer-Verlag, New York, 1989).
 - [4] J. E. Marsden and T. S. Ratiu, *Introduction to Mechanics and Symmetry* (Springer-Verlag, Berlin, 1994).
 - [5] V. I. Arnold and B. A. Khesin, *Topological Methods in Hydrodynamics* (Springer-Verlag, New York, 1998).
 - [6] Y. Watanabe, *Physica D* **225**, 197 (2007).
 - [7] R. M. Wald, *General Relativity* (University of Chicago Press, Chicago, 1984).

- [8] S. W. Rienstra, *ZAMM* **76**, 423 (1996).
- [9] C. M. Edwards, S. D. Howison, H. Ockendon and J. R. Ockendon, *IMA J. Appl. Math.* (2007), in press.
- [10] F. Bouchut, On zero pressure gas dynamics, in *Advances in Kinetic Theory and Computing*, ed. B. Perthame, Advances in Mathematics for Applied Sciences, Vol. 22 (World Scientific, 1994).
- [11] J. Li, T. Zhang and S. Yang, *Two-dimensional Riemann Problems in Gas Dynamics* (Chapman & Hall/CRC Press, Boca Raton, FL, 1998).
- [12] H. Yang, *J. Diff. Eqns.* **159**, 447 (1999).
- [13] J. Li, *Appl. Math. Lett.* **14**, 519 (2001).
- [14] I. Kreyszig, *Differential Geometry* (University of Toronto Press, Toronto, 1959).
- [15] H. Flanders, *Differential Forms with Applications to the Physical Sciences* (Dover, New York, 1990).
- [16] J. L. Synge and A. Schild, *Tensor Calculus* (Dover, New York, 1978).
- [17] B. Schutz, *Differential Geometry* (Cambridge University Press, Cambridge, U.K., 1980).
- [18] J.-L. Thiffeault, *J. Phys. A* **34**, 5875 (2001).
- [19] For a step-by-step derivation of the geodesic deviation equation see <http://io.uwinnipeg.ca/~vincent/4500.6-001/Cosmology/GeodesicDeviation.htm>.
- [20] J.-L. Thiffeault and K. Kamhawi, <http://arXiv.org/abs/nlin/0607075> (2006).